FIRST LOOK AT THE FOMALHAUT DEBRIS DISK WITH THE SPITZER SPACE TELESCOPE[1]

K. R. STAPELFELDT,[2] E. K. HOLMES,[2,3,4] C. CHEN,[2,3] G. H. RIEKE,[5] K. Y. L. SU,[5] D. C. HINES,[5,6] M. W. WERNER,[2] C. A. BEICHMAN,[2] M. JURA,[7] D. L. PADGETT,[8] J. A. STANSBERRY,[5] G. BENDO,[5] J. CADIEN,[5] M. MARENGO,[9] T. THOMPSON,[2] T. VELUSAMY,[2] C. BACKUS,[2] M. BLAYLOCK,[5] E. EGAMI,[5] C. W. ENGELBRACHT,[5] D. T. FRAYER,[8] K. D. GORDON,[5] J. KEENE,[2,8] W. B. LATTER,[8] T. MEGEATH,[9] K. MISSELT,[5] J. E. MORRISON,[5] J. MUZEROLLE,[5] A. NORIEGA-CRESPO,[8] J. VAN CLEVE,[10] AND E. T. YOUNG[5]

ABSTRACT

We present *Spitzer Space Telescope* early release observations of Fomalhaut, a nearby A-type star with dusty circumstellar debris. The disk is spatially resolved at 24, 70, and 160 μm using the Multiband Imaging Photometer for *Spitzer* (MIPS). While the disk orientation and outer radius are comparable to values measured in the submillimeter, the disk inner radius cannot be precisely defined: the central hole in the submillimeter ring is at least partially filled with emission from warm dust, seen in *Spitzer* Infrared Spectrograph (IRS) 17.5–34 μm spectra and MIPS 24 μm images. The disk surface brightness becomes increasingly asymmetric toward shorter wavelengths, with the south-southeast ansa always brighter than the north-northwest one. This asymmetry may reflect perturbations on the disk by an unseen interior planet.

Subject headings: circumstellar matter — infrared: stars — planetary systems — stars: individual (Fomalhaut)

1. INTRODUCTION

Fomalhaut (α Pisces Austrinus; GJ 881; HIP 113368; IRAS 22549−2953) is a bright ($V = 1.2$) A3 V star only 7.7 pc distant. Attention was focused on this system because of discovery by the *Infrared Astronomical Satellite* (*IRAS*) of a large far-infrared excess, indicative of circumstellar dust with a temperature of $\sim$75 K (Aumann 1985). Given the main-sequence age of the star ($\sim$200 Myr; Barrado y Navascués 1998), this dust could not be primordial, as it would have been removed by radiation pressure and Poynting-Robertson drag on relatively short timescales; recent dust production from collisions between larger parent bodies is required (Backman & Paresce 1993). Optical imaging searches failed to detect the suspected disk in scattered light (Smith et al. 1992; Kalas & Jewitt 1996), but it was finally resolved in the far-IR by Harvey et al. (1996) and in submillimeter maps by Holland et al. (1998). At 850 μm, the morphology is that of a ring or torus $\sim$36″ (280 AU) in diameter and inclined $\sim$20° from edge-on (Dent et al. 2000). Subsequent mapping at 450 μm revealed a ring brightness asymmetry that has been interpreted as a dense clump between the ring ansae (Holland et al. 2003), and which might be dust that is dynamically trapped in resonance with a perturbing object (Wyatt & Dent 2002).

Spitzer (Werner et al. 2004) brings new levels of sensitivity and spatial resolution to debris disk studies in the thermal infrared. This paper reports initial results for Fomalhaut, the first debris disk target to be spatially resolved in the *Spitzer* science mission.

2. OBSERVATIONS

Fomalhaut images were obtained on 2003 November 19 with the Multiband Imaging Photometer for *Spitzer* (MIPS; Rieke et al. 2004). Multiple dithered 3 s exposures were obtained using the 24 μm, 70 μm (default and fine scale), and 160 μm channels in the small-field mode of the MIPS photometry astronomical observing template (AOT). The 24 and 70 μm dither patterns were each executed four times on a square grid of 3.25×3.25 pixels in x, y array coordinates, providing a high degree of subpixel sampling to facilitate point-spread function (PSF) subtraction and deconvolutions. The total integration time on-source was 192 s for 24 μm, 60 s for 70 μm default scale, 192 s for 70 μm fine scale, and 162 s for 160 μm. A PSF standard (HD 217382) was also observed at 24 μm, using the identical observing strategy.

The MIPS instrument team's Data Analysis Tool (DAT; Gordon et al. 2004) was used to perform the basic data reduction. The 24 μm images were further processed to remove a vertical "jail bar" pattern that appears during observations of bright sources. The MIPS 160 μm camera suffers from a spectral leak in which stray light in the wavelength range of 1–1.6 μm produces a second source image offset from the true 160 μm source. Images of the unresolved K0 giant HD 197989 were scaled and subtracted from the Fomalhaut image to remove both the spectral leak image artifact and the small ($\sim$60 mJy) photospheric component of Fomalhaut's 160 μm image.

Mid-infrared spectra of Fomalhaut were obtained on 2003 November 23 with *Spitzer*'s Infrared Spectrograph (IRS) instrument (Houck et al. 2004). Measurements were made with the staring AOT and the Long-Low (LL) module, which provides $R \approx 64-128$ over the wavelength range of 14–37 μm. Two positions were observed: directly on the star, and a location 17″ to the south-southeast (on the ansa of the submillimeter ring). Spacecraft pointing was peaked up using IRS

[2] Jet Propulsion Laboratory, California Institute of Technology, 4800 Oak Grove Drive, Pasadena, CA 91109; krs@exoplanet.jpl.nasa.gov.

[3] National Research Council Resident Research Associate.

[4] Deceased March 23, 2004.

[5] Steward Observatory, University of Arizona, 933 North Cherry Avenue, Tucson, AZ 85721.

[6] Space Science Institute, 4750 Walnut Street, Suite 205, Boulder, CO 80301.

[7] Department of Physics and Astronomy, University of California, Los Angeles, CA 90095.

[8] *Spitzer* Science Center, California Institute of Technology, Pasadena, CA 91125.

[9] Harvard-Smithsonian Center for Astrophysics, 60 Garden Street, Cambridge, MA 02138.

[10] Ball Aerospace Corporation, 1600 Commerce Street, Boulder, CO 80301.

images of a nearby star, placing the requested target position within 0″4 of the center of the 10″6″ × 168″ long slit. The two slit positions and their orientation are shown overlaid on the 24 μm image in Figure 2a. Two 6 s ramp exposures were made at each of the two slit positions in each spectrograph module.

The IRS *droopres* product from the *Spitzer* Science Center's S9.1 pipeline was loaded in the IRS team's SMART IDL software environment (Higdon et al. 2004). The long-slit spectra were calibrated and extracted following procedures described by Uchida et al. (2004). A 100″ long aperture was used for extraction at the ansa position. Alpha Lac (type A1 V) was used as a standard for the instrument relative spectral response. The final spectra were multiplied by a factor of 0.828 to make them consistent with the MIPS 24 μm and *IRAS* 25 μm flux densities of Fomalhaut (see § 3.2 below).

3. RESULTS

3.1. *Spectroscopy*

The IRS low-resolution spectrum of Fomalhaut is shown in the top panel of Figure 1. At the stellar position (*upper curve*), the spectrum is saturated for all $\lambda < 17.5$ μm (not shown). Only instrumental artifacts appear superposed on an otherwise featureless continuum spectrum; future calibration improvements will allow limits to be set on the strength of spectral features in this wavelength range. The spectral slope is not Rayleigh-Jeans at any wavelength: the spectral index ranges from -1.65 between 17.5 and 20 μm, to -1.1 between 21 and 28 μm (the bandpass of the MIPS 24 μm camera), and $+0.5$ between 30 and 35 μm. This is the first detection of an infrared excess for Fomalhaut at $\lambda < 25$ μm. To quantify the magnitude of this excess, an A3 V Kurucz model atmosphere with $[\mathrm{Fe/H}] = 0.05$ (Lejeune et al. 1997) was fitted to the photospheric fluxes. This model, with a reduced $\chi^2 = 0.96$, is plotted along with the data points in the bottom panel of Figure 1 and was subtracted from the *Spitzer* IRS spectrum to give the infrared excess versus wavelength (top panel of Fig. 1, *middle curve*). Between 20 and 30 μm, the excess increases linearly with λ. The spectrum on the south-southeast ring ansa (top panel of Fig. 1, *bottom curve*) combines local disk emission with the diffraction wings of the central source. It declines from 16 to 22 μm and then begins to rise continuously toward longer wavelengths. This behavior is broadly consistent with the expected spectrum of the PSF wings at the ansa position (when weighted by the measured brightness of the central source); disk emission from the ansa position must therefore be quite faint at these wavelengths. Together, the spectra in Figure 1 clearly identify a new component of warm ($T \approx 150$ K) dust concentrated in the center of the Fomalhaut debris system.

3.2. *Photometry*

Background-subtracted flux densities were measured for Fomalhaut in a 50″ diameter circular aperture at 24 μm, and in elliptical apertures oriented along the disk major axis, with sizes of 64″ × 45″ and 41″ × 29″ at 70 and 160 μm, respectively. Aperture corrections were applied to these results using model PSFs produced by version 1.3 of the *Spitzer* Tiny Tim software (Krist 2002). At 24 μm, the Fomalhaut system flux density was found to be 3.90 ± 0.04 Jy, corrected to an equivalent monochromatic value at 23.68 μm. In addition to the random errors, there is a possible ~10% error bar in absolute calibration. The MIPS 24 μm result agrees well with the color-corrected *IRAS* 25 μm flux density of 3.85 ± 0.3 Jy (Beichman et al. 1988). We also found total system flux
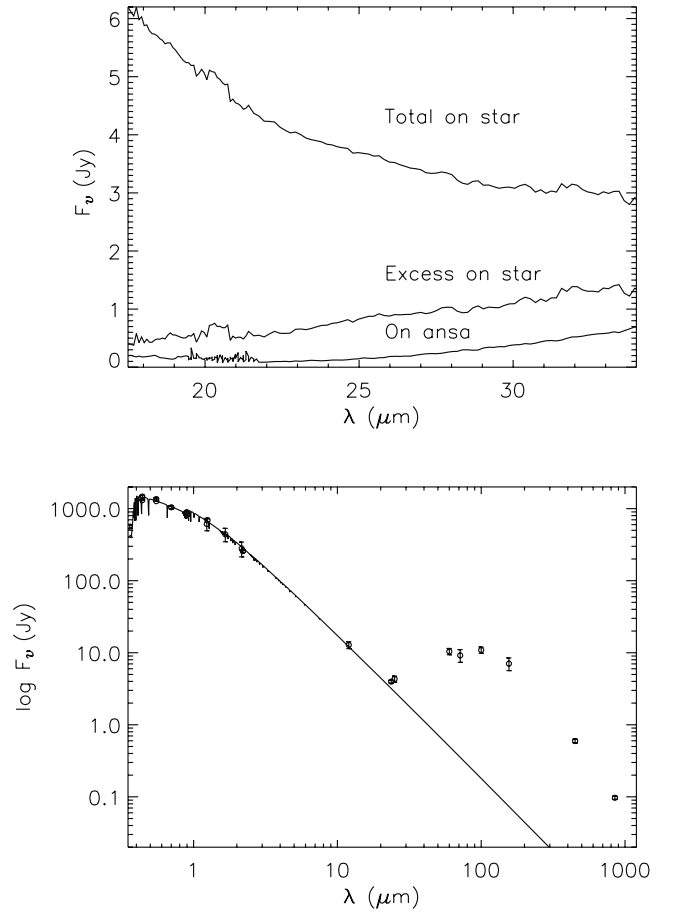

Fig. 1.—Spectral data for Fomalhaut. *Top panel*: IRS Long-Low spectrum of Fomalhaut on the stellar position (*top curve*); the same spectrum with the best-fit A3 V Kurucz model photosphere subtracted (*middle curve*); and a spectrum taken 17″ south-southeast of the star, on one ansa of the submillimeter ring (*bottom curve*). *Bottom panel*: Star's spectral energy distribution. The optical and near-IR data points are taken from Johnson et al. (1966) and Glass (1974); the infrared points are new MIPS measurements and data from the *IRAS* Point Source Catalog; and the submillimeter data is from Holland et al. (2003). The solid curve shows the Kurucz model fit to the $\lambda < 10$ μm data points.

densities of 9.2 ± 1.8 Jy and 7.0 ± 2.8 Jy at 70 and 160 μm, respectively.

The measured 24 μm flux density can be used to better quantify the excess emission already indicated in this wavelength region by the IRS results. The Kurucz model fit (see bottom panel of Fig. 1) predicts 3.24 Jy for the photosphere at 23.68 μm, implying a 0.66 Jy excess at this wavelength. Kurucz model predictions for a suite of MIPS 24 μm standard stars provide the fundamental flux calibration of the instrument. Given that the same method is used for Fomalhaut and for the standards, relative errors between the measurements should be small, and thus Fomalhaut's measured excess should be robust against systematic errors. An independent estimate of the excess can be made using *IRAS* data.

For a sample of seven A-type stars with high-quality near-IR photometry and no 60 μm excess (HD 60178, 130841, 80007, 48915, 11636, 103287, and 110304), the average $K - [25 \ \mu m]$ flux density ratio is 70.18. No color corrections were applied to the *IRAS* data, so this ratio can be taken as an empirical color. Fomalhaut is redder than this average ratio by an amount equivalent to a color-corrected excess of 0.71 ± 0.18 Jy at 25 μm. The two estimates are consistent with the presence of 0.7 ± 0.2 Jy of 24 μm excess emission.

3.3. *MIPS Imaging*

The direct 24 μm image of Fomalhaut (Fig. 2a [Plate 1]) is dominated by the PSF of the bright central point source. By aligning, scaling, and subtracting the reference PSF image from that of Fomalhaut, the central source can be completely removed, and any extended emission clearly seen. In this central-source-subtracted image (Fig. 2b), two ~20″ extensions of excess emission are clearly detected along P.A. 150° and 330°. This emission is oriented identically along the major axis of the submillimeter continuum structure (Holland et al. 2003) and has virtually the same radial extent. It is more smoothly distributed than the submillimeter excess emission, with no sign of bright peaks at the ring ansa locations. In addition, the south-southeast extension has ~50% greater surface brightness than at corresponding radii on the north-northeast extension. We conclude that this extended 24 μm excess traces disk material on, and possibly interior to, the submillimeter ring. However, this extended emission comprises only a small part of Fomalhaut's total 24 μm excess. Excluding the central region $r < 10''$, which is dominated by PSF-subtraction residuals, the flux in the extended disk is only 0.13 ± 0.02 Jy, while the total excess is 4–7 times larger. The remaining excess must arise from very near the central star. Repeating the PSF subtraction, but now scaling the reference PSF to the flux density indicated by our Kurucz model fit, the result (Fig. 2c) shows a bright, compact excess of 0.6 ± 0.2 Jy at the stellar position, in accord with the spectroscopic finding of a central warm excess (§ 3.1).

At 70 μm, Fomalhaut appears as a bar of emission elongated ~40″ along P.A. 150° (the same P.A. as the 24 μm extended emission, and the submillimeter ring) and asymmetrically bright on its south-southeast end (Figs. 2d and 2e). The expected photospheric emission is only 0.3 Jy, less than 5% of the measured flux density, and indeed no central point source can be identified in the MIPS images. The bar of 70 μm emission is centered on the FK5 stellar position to within the astrometric uncertainties (currently 3″ for the 70 μm fine-scale mode). To provide an improved view of the disk, the set of fine-scale dithered images (Fig. 2e) was mosaicked and deconvolved using 20 iterations of the HIRES algorithm (Aumann et al. 1990) and a Tiny Tim model PSF. In this reconstruction (Fig. 2f), two disk ansae corresponding to those of the submillimeter ring are confirmed. The south-southeast ansa has a surface brightness that is ~30% larger than the north-northwest ansa, and is also more extended inward toward the star. This asymmetry is reminiscent of the more subtle (~5%) one seen in 450 μm maps (Holland et al. 2003). Comparable deconvolution results were obtained using an independent maximum-entropy (MEM) algorithm.

The 160 μm emission from Fomalhaut (Figs. 2g and 2h) is also elongated along P.A. 150°, but with an extent only 50% larger than *Spitzer*'s diffraction-limited beam size. The leak-subtracted 160 μm mosaic was deconvolved using 80 iterations of the HIRES algorithm and a Tiny Tim model PSF. The result (Fig. 2i) also reveals two emission peaks on the ansae of the submillimeter ring, with the south-southeast ansa again brighter than the north-northwest one, but now by only ~10%. As at 70 μm, an independent MEM deconvolution produced comparable results.

4. DISCUSSION

The new *Spitzer* data provide convincing evidence for a component of warm dust at radii under 100 AU, interior to the
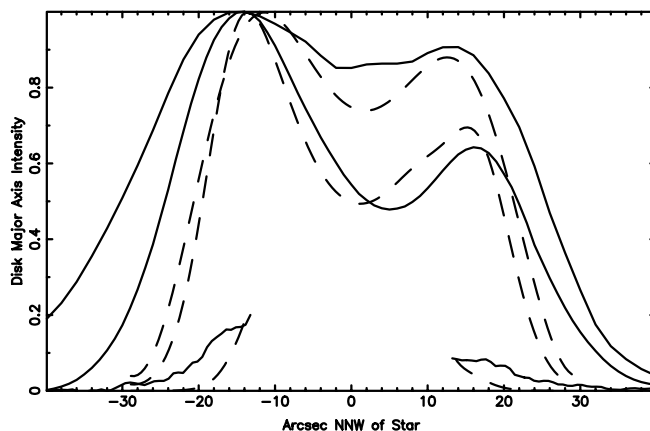

Fig. 3.—Line cuts through the MIPS images and disk models. The images used were taken from Figs. 2b, 2f, and 2i. The flux is extracted as a function of position along the disk major axis P.A. of 150°, and binned in a 30″ wide aperture perpendicular to the disk. A median background level was subtracted. The line cuts through the 160, 70, and 24 μm images are plotted as the upper, middle, and lower solid curves, respectively. The central region of the 24 μm curve, which is dominated by PSF subtraction residuals, has been blanked out. The dashed curves show line cuts of 160, 70, and 24 μm emission (*from top to bottom*) from an offset disk model that has been convolved with the MIPS PSF (see text).

submillimeter ring. The low-resolution spectrum shows strong excess emission from 17 to 35 μm on the stellar position, while at the ansa position the excess emission is much weaker. Furthermore, subtraction of a best-estimate photospheric point source from the center of the MIPS 24 μm image reveals a region of compact residual excess emission extending inward to the limit of our spatial resolution ($r < 20$ AU). It is difficult to uniquely determine the spatial distribution of this inner warm dust, given *Spitzer*'s diffraction limit, the residual artifacts of PSF subtraction, and the remaining uncertainty in the magnitude of the 24 μm excess. It is not clear from the 24 μm image if the emitting dust extends continuously inward from the outer ring, or if a separate dust source region is present close to the star. The slope of the spectrum between 20 and 30 μm is consistent with a $1/r$ radial density distribution and the inward drift of grains from the outer ring (Buitrago & Mediavilla 1985), whereas the 24 μm source compactness suggests the possibility of a second dust source region in an inner asteroid belt at $r < 20$ AU. In either case, the absence of any compact central emission in submillimeter maps (Holland et al. 2003) requires that Fomalhaut's inner dust cloud be relatively tenuous, with an optical depth less than 10% of that of the outer dust ring. The presence of an inner disk of warm dust was similarly shown for β Pictoris from ground-based observations (Backman et al. 1992).

The asymmetry seen in the MIPS images of the Fomalhaut disk is intriguing. A key property is that its strength changes with wavelength, or equivalently, with orbital distance from the central star. Figure 3 shows line cuts along the disk major axis for all three MIPS images. At 160 μm, the brightness asymmetry (maximum/minimum surface brightness) between the two ansae is about 10%; at 70 μm, it is about 30%. At 24 μm, no ansae are visible, but at their radial position the surface brightness asymmetry is about 50%. Finally, it is notable that the 70 μm asymmetry is morphological as well as radiometric: the south-southeast ansa is broader and more extended inward toward the star than the north-northwest ansa. This, and the asymmetry's greater strength at shorter

wavelengths, suggests an origin in warmer material at or interior to the inner edge of the submillimeter ring.

In the case of circular orbits for both the massive outer dust ring and the tenuous inner disk, the surface brightness asymmetry must arise via a density enhancement near the ring's inner edge. A recent asteroid collision releasing a localized cloud of particles might account for this. Such collisions must be taking place in order to continuously replenish the disk dust population against radiation-driven loss mechanisms. However, the dust cloud from such a collision would disperse smoothly into the overall disk on a few orbital timescales ($\sim 10^4$ yr). Thus, this model requires that we view the disk at a special time after a major recent collision. Wyatt & Dent (2002) argue that such collisions should be rare, unless planetesimal formation has occurred very recently in the system. Alternatively, a disk density enhancement could be dynamically maintained by mean motion resonances with a perturbing planet (Quillen & Thorndike 2002; Holmes et al. 2003; Kuchner & Holman 2003). In this case, dust particles become trapped in regions of orbital phase space that have low-order resonances ($2:1$, $3:2$, etc.) with the orbital period of the perturbing object. However, in this model the trapped dust is restricted to a relatively narrow range of orbital periods (distances) with the required commensurability. The wavelength dependence of the asymmetry, and its apparent inward radial extent in the MIPS 70 μm image, may therefore be difficult to account for with this model.

Another origin for the asymmetry could be that the outer dust ring and inner disk are actually noncircular, with the star displaced from the ring center. This situation could arise if a planetary perturber on an eccentric orbit lies interior to the bright ring. The ring would acquire a forced eccentricity, with the periastron longitude of dust particle orbits becoming preferentially aligned with that of the perturber. An asymmetry in the ring thermal emission would then arise from the warmer dust particles at periastron (Wyatt et al. 1999). In this model, a ring eccentricity $e = 0.07$ would be sufficient to reproduce the observed 70 μm surface brightness asymmetry. This e is sufficiently small that the stellar offset from the ring center, and the ring's eccentric shape, would not be distinguished from a centered circular ring in our images. Furthermore, in this model the dust particle orbits would be more eccentric in the inner parts of the disk nearer the perturber and less eccentric in the outer disk regions more distant from the perturber. This model therefore accounts well for the observed increase in the asymmetry toward shorter wavelengths. Models of such a system using low-order secular perturbation theory, placing a single planet with $a = 40$ AU, $e = 0.15$ inside a partially filled dust ring, produce model disk brightness profiles similar to the observed wavelength-dependent asymmetry. Line cuts through these models are compared to the data in Figure 3.

The nature of the perturbing body is difficult to infer, because of *Spitzer*'s low resolution and the relative insensitivity of the models to the mass and orbital parameters of the perturber. However, the presence of numerous signatures of planets seen in the diffuse emission from dust in our own solar system (Dermott et al. 1998) makes this a compelling paradigm for other solar systems (Holmes 2002; Holmes et al. 2003).

REFERENCES

Aumann, H. H. 1985, PASP, 97, 885
Aumann, H. H., Fowler, J. W., & Melnyk, M. 1990, AJ, 99, 1674
Backman, D. E., & Paresce, F. 1993, in Protostars and Planets III, ed. E. H. Levy, J. I. Lunine, & M. S. Matthews (Tucson: Univ. Arizona Press), 1253
Backman, D. E., Witteborn, F., & Gillett, F. 1992, ApJ, 385, 670
Barrado y Navascués, D. 1998, A&A, 339, 831
Beichman, C. A., et al., ed. 1988, *IRAS* Catalogs and Atlases: Explanatory Supplement (NASA RP-1190; Washington: GPO)
Buitrago, J., & Mediavilla, E. 1985, A&A, 148, L8
Dent, W. R. F., et al. 2000, MNRAS, 314, 702
Dermott, S. F., Grogan, K., Holmes, E. K., & Wyatt, M. C. 1998, in Exozodiacal Dust Workshop Proceedings, ed. D. E. Backman, L. J. Caroff, S. A. Sandford, & D. H. Wooden (Moffett Field: NASA), 59
Glass, I. S. 1974, Mon. Notes Astron. Soc. South Africa, 33, 53
Gordon, K. D., et al. 2004, PASP, submitted
Harvey, P. M., et al. 1996, ApJ, 471, 973
Higdon, S. J. U., et al. 2004, PASP, submitted
Holland, W. S., et al. 2003, ApJ, 582, 1141

Holland, W. S., et al. 1998, Nature, 392, 788
Holmes, E. K. 2002, Ph.D. thesis, Univ. Florida
Holmes, E. K., et al. 2003, ApJ, 597, 1211
Houck, J. R., et al. 2004, ApJS, 154, 18
Johnson, H. L., Iriarte B., Mitchell R. I., & Wisniewski W. Z. 1966, Comm. Lunar Planet Lab., 4, 99
Kalas, P., & Jewitt, D. 1996, AJ, 111, 1347
Krist, J. 2002, Tiny Tim/SIRTF User's Guide (Pasadena: SSC)
Kuchner, M. J., & Holman, M. J. 2003, ApJ, 588, 1110
Lejeune, T, Cuisinier, F., & Buser, R. 1997, A&AS, 125, 229
Quillen, A. C., & Thorndike, S. 2002, ApJ, 578, L149
Rieke, G., et al. 2004, ApJS, 154, 25
Smith, B. A., Fountain, J., & Terrile, R. 1992, A&A, 261, 499
Uchida, K., et al. 2004, ApJS, 154, 439
Werner, M. W., et al. 2004, ApJS, 154, 1
Wyatt, M. C., & Dent, W. R. F. 2002, MNRAS, 334, 589
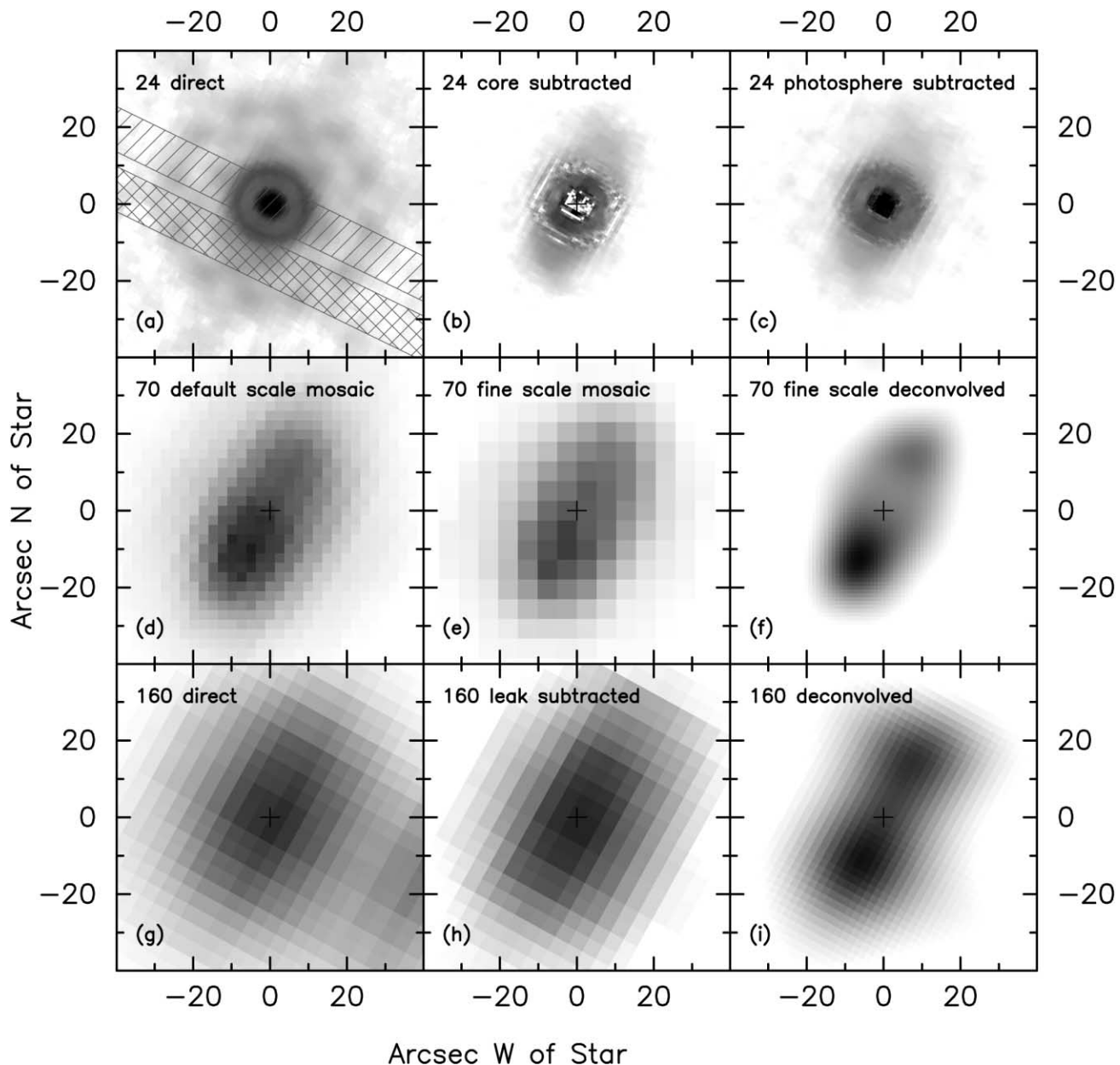Wyatt, M. C., et al. 1999, ApJ, 527, 918

Fig. 2.—Images of Fomalhaut in the three MIPS channels. North is up and east is to the left in all the panels, and $10'' = 77$ AU at Fomalhaut's distance. Images in the left-hand column—(*a*), (*d*), and (*g*)—have been reconstructed from multiple dithered exposures, and are oversampled by a factor of 4. *Top row*: 24 μm images in log stretch; (*a*) is the direct image, dominated by the stellar PSF, with the two IRS LL slit positions are overlaid; (*b*) shows this image with a reference PSF subtracted to remove all of the central point source emission; and in (*c*), the subtracted PSF is scaled by the expected stellar photospheric flux density, and reveals a compact region of 24 μm excess very near the star. The FWHM of the MIPS 24 μm PSF is 5.''4. *Middle row*: 70 μm images in linear stretch; (*d*) is the default scale image used for photometric measurements; (*e*) shows the fine scale image; and (*f*) shows the deconvolution of the fine-scale image using 20 iterations of the HIRES algorithm. The FWHM of the MIPS 70 μm PSF is $16''$. *Bottom row*: 160 μm images in linear stretch; (*g*) is the direct image; (*h*) shows this image after subtraction of the adjacent ghost arising from the spectral leak; and (*i*) shows a deconvolution of the leak-subtracted image with 80 iterations of the HIRES algorithm. The FWHM of the MIPS 160 μm PSF is $35''$.

PLATE 1